International Journal of Refrigeration 168 (2024) 334–344

Contents lists available at ScienceDirect

International Journal of Refrigeration

journal homepage: www.elsevier.com/locate/ijrefrig

Theoretical analysis of the optimal ejector operation and design within an ejector-based refrigeration system

Analyse théorique du fonctionnement et du design optimaux de l'éjecteur dans un système de réfrigération à éjecteur

Antoine Metsue [a,b,*], Hakim Nesreddine [c], Yann Bartosiewicz [b], Sébastien Poncet [a]

[a] *Mechanical Engineering Department, Université de Sherbrooke, Sherbrooke (QC), Canada*
[b] *Institute Mechanics, Materials, and Civil Engineering (iMMC), Université catholique de Louvain, Louvain-la-Neuve, Belgium*
[c] *Laboratoire des technologies de l'énergie, Hydro-Québec, Shawinigan (QC), Canada*

ARTICLE INFO

Keywords:
Carbon dioxide
Refrigeration cycle
Transcritical ejector
Coefficient of performance
Design

Mots clés:
Dioxyde de carbone
Cycle de réfrigération
Éjecteur transcritique
Coefficient de performance
Design

ABSTRACT

Optimal operation and design of ejectors are the subject of recent concerns, especially for the enhancement of refrigeration and heat pump cycles based on natural refrigerants like carbon dioxide. In this study, a thermodynamic analysis of an ejector-based refrigeration cycle is performed to determine both what operating pressures lead to the highest physically possible performance depending on the ambient conditions, and what are the main dimensions of the ejector leading to the best performance at a given ambient temperature. A state-of-the-art thermodynamic model for the prediction of the ejector performance is for the first time utilized to generate reliable operation and performance maps of the ejector cycle. Most notably, it is found that the optimal coefficient of performance is not necessarily found when the ejector operates at critical conditions but mostly when the device is under off-design regime, depending on the ejector internal efficiency and the hot side temperature. In addition, the analysis reveals that the performance of the cycle is not highly sensitive to the throat area ratio of the ejector given that the latter lies within an acceptable range. Those findings contribute to getting a better understanding of how the cycle benefits from the ejector and define design and control strategies for the cycle.

1. Introduction

Ejector refrigeration systems (ERSs) are becoming a compelling alternative to the classical refrigeration cycle since these systems can recover part of the exergy losses that occur at the expansion level. Originally motivated by the transition towards natural refrigerants that tend to have lesser performances than fluorocarbons (CFCs, HCFCs and HFCs), the integration and optimal operation of the ejector within the refrigeration system are now the subject of many works (see in Besagni et al., 2016). Carbon dioxide (CO_2) has emerged as an appealing choice for a working fluid due to its non-toxic and non-flammable properties. Additionally, the shift towards CO_2 utilization has been driven by international agreements like the Kyoto Protocol, which mandates phased reductions in the use of HCFCs and HFCs within the next two decades (Abas et al., 2018). In Europe, the revised F-gas regulation aims at reducing the EU's fluorinated greenhouse gas emissions by two-thirds by 2030.

Because carbon dioxide has a critical temperature of 31 [°C], the cycle must often operate under *transcritical* conditions depending on the ambient temperature. However, operating at higher temperatures requires high compression of the refrigerant, which quickly introduces notable losses in the expansion valve due to the high pressure ratio (Kim et al., 2004) and the higher entropy production of CO_2 during the isenthalpic expansion compared to classical refrigerants (Elbel and Lawrence, 2016). The design of CO_2 ejectors and the optimal operation of the CO_2 ERS are therefore subject of recent concerns for the enhancement of the performance of the refrigeration systems (Besagni, 2019). Yet, ejectors are known to have intricate fluid dynamics, and it is the authors' opinion that certain underlying mechanisms within these devices (e.g., the double choking mechanism) remain not fully understood and often poorly modeled, which may lead to sub-optimal ejector design and contributes to hamper operation strategies of the ERS.

* Corresponding author at: Institute Mechanics, Materials, and Civil Engineering (iMMC), Université catholique de Louvain, Louvain-la-Neuve, Belgium.
E-mail address: antoine.metsue@uclouvain.be (A. Metsue).

https://doi.org/10.1016/j.ijrefrig.2024.09.020
Received 2 April 2024; Received in revised form 31 July 2024; Accepted 18 September 2024
Available online 24 September 2024
0140-7007/© 2024 Elsevier Ltd and IIR. All rights are reserved, including those for text and data mining, AI training, and similar technologies.

Nomenclature

Alpha numeric symbols

$\dot{Q}$	Heat power (W)
$\dot{W}$	Work power (W)
A	Area (m^2)
h	Specific enthalpy (J kg^{-1})
p	Pressure (Pa)
s	Specific entropy (J kg^{-1} K^{-1})
T	Temperature (K)
x	Quality (-)

Subscripts

amb	Ambient
comp	Compressor
cool	Cooling
crit	Critical point
d	Diffuser outlet
e	Primary nozzle exit
ev	Evaporator
gc	Gas cooler
m	Mixed flow
out	Ejector outlet conditions
p	Primary flow
s	Secondary flow
sat	Saturated conditions
t	Primary nozzle throat
y	Hypothetical throat

Greek letters

η	Efficiency (-)
ω	Entrainment ratio (-)

In 1931, Gay (1931) first proposed the basic transcritical CO_2 ejector refrigeration system (as shown in Fig. 1, Section 2.1). This configuration has since been demonstrated to yield the highest coefficient of performance (COP) and exergy efficiency among the proposed layouts for CO_2 systems (Taslimi Taleghani et al., 2018). The high pressure supercritical CO_2 coming from the gas cooler is expanded in the ejector, thereby pre-compressing the gas CO_2 coming from the evaporator, and the refrigerant thus has an intermediate pressure at the compressor inlet, so that the compressor can operate at a lower charge. In addition, the ejector can improve the evaporator performance due to the consequently near-liquid feeding operation (Pottker and Hrnjak, 2015). In 1990, Kornhauser (1990) performed a first analysis of cycle performance using a simple in-house ejector heat pump model that was implemented as a FORTRAN routine. The author (Kornhauser, 1990) compared the performance of a standard vapor compression cycle and an ERS for different refrigerants and found potential COP improvements ranging from 12% to 30%. Nehdi et al. (2007) later developed a computer code that uses fluid properties retrieved from NIST REFPROP to evaluate the influence of the ejector area ratios on the cycle performance. The analysis was performed for several refrigerants and it was concluded that a maximum COP improvement of 22% could be achieved by using an ejector in R141b systems, which was the most favorable case. Bilir Sag et al. (Bilir and Ersoy, 2009) used a similar routine to investigate the two-phase R134a ERS and found a similar range of potential COP improvement. In addition, the authors (Bilir and Ersoy, 2009) noted that even if the ejector worked under off-design regime, the cycle performance still benefited from the ejector. Several similar studies have been subsequently performed to investigate the influence of the ejector on the cycle performance (Sarkar, 2010; Li et al., 2014; Zhao et al., 2015; Khosravi et al., 2018).

In 2005, Li and Groll (2005) studied the influence of operating parameters on the COP of the CO_2 cycle. Most notably, the authors found that the COP of the ERS could be improved by more than 16% over the basic transcritical cycle, for typical air conditioning operating conditions. Several theoretical works have later been done to assess the performance of the CO_2 ERS specifically (Ksayer and Clodic, 2006; Deng et al., 2007; Fangtian and Yitai, 2011; Zhang and Tian, 2014; Zheng et al., 2015). Notably, Fangtian and Yitai (2011) performed an exergy analysis to evaluate the losses in the different parts of the cycle and found that there exists a critical entrainment ratio, a critical gas cooler outlet temperature and an optimal heat rejection pressure that optimize the cycle operation. Some studies then focused on modifying the geometry of the ejector itself to be able to match the optimal operating conditions as closely as possible. Elbel and Hrnjak (2008) found out that regulating the high-side pressure with an ejector needle could be a way of optimizing the cycle performance, much as for a traditional expansion valve cycle. Alternatively, multi-ejector systems received growing interest in the recent years and are already commercialized in the form of ejector packs that comprise cartridges containing several ejectors of different sizes and internal geometries. Depending on the operating conditions, some ejectors are then activated through the action of solenoid valves (Banasiak et al., 2015; Singh et al., 2021).

Some recent studies (Chen et al., 2021; Liu et al., 2020, 2012, 2018) have also opted to use the Dymola commercial software, that allows to perform transient operation analyses with out-of-the-box components models available in commercial libraries. Recently, Metsue et al. (2021) investigated the influence of the ejector geometry on the performance of a transcritical CO_2 ejector cycle using Dymola. The authors used their in-house ejector model (Metsue et al., 2022) calibrated onto the CO_2 experimental data of Zhu et al. (2017) and found that there exists an ejector size that maximizes the COP of the cycle, and that critical ejector pressure is not reached at this optimum COP point. Rather, the ejector is operating well under the on-design regime.

Nonetheless, the authors believe that a deep understanding of the link between ejector operating regime and overall cycle performance is still lacking. Yet, this knowledge is fundamental to set up efficient design strategies at the component level and determine adequate cycle operation strategies. In this study, the classical CO_2 ERS is analyzed theoretically to give insight onto the optimal operation pressures of the cycle. To this end, a typical refrigeration application (e.g., air conditioning) is considered. The operation of the ejector is predicted using the state-of-the-art ejector thermodynamic model of Metsue et al. (2022), that integrates the natural physics of the compound-choking theory for predicting double-choking operation. This allows to establish the domain of operation that is allowable by the physics and determine the operating pressures that yield the highest coefficient of performance. A parametric analysis of the secondary to primary throat area ratio of the device is also carried out to find the optimal ejector dimensions for specific operation temperatures and determine the sensitivity of the COP to this geometrical parameter. The link between the cycle performance and the operating regime of the ejector is investigated, and the effects of the entropy-generating mixing phenomena within the device are highlighted.

2. Thermodynamic modeling

The numerical modeling of the ejector cycle is here described. In Section 2.1, the system is first solved assuming an ejector that can provide any performance required by the cycle. In Section 2.2, the ejector entrainment ratio is then calculated with the real ejector thermodynamic model to determine the actual possible operation of the device (i.e., that could also be allowed to fulfill the physical conditions).

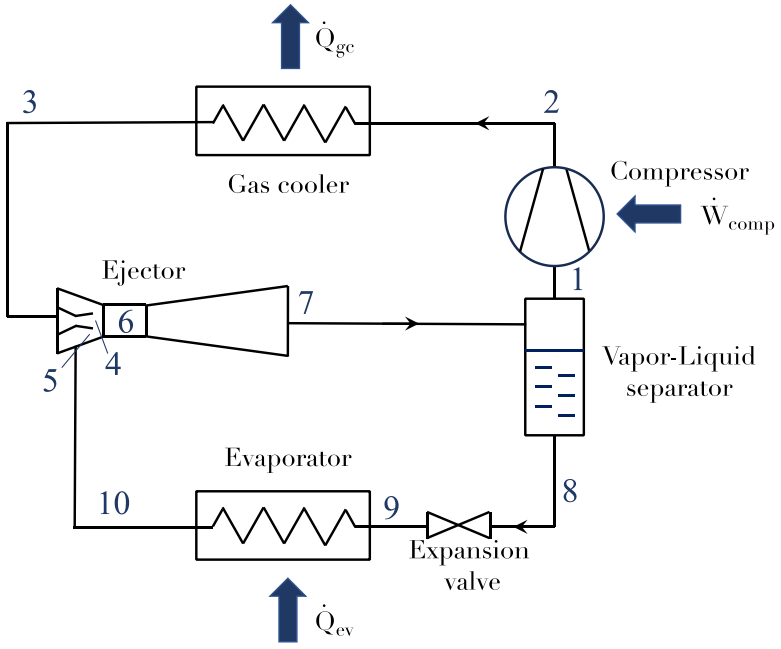

Fig. 1. Classical ejector refrigeration system. The main locations of the cycle have been numbered for reference within the text.

2.1. Cycle modeling

As stated in the previous section, the present work focuses on the analysis of the classical refrigeration cycle shown in Fig. 1. The system is modeled with the following assumptions:

- The cycle operates in steady state.
- The ambient temperature T_{amb} (external) is fixed. Three values of T_{amb} will be considered in the following: 15, 25 and 35 [°C].
- The cooling temperature (external) is fixed to $T_{cool} = 4$ [°C].
- The pinch temperatures at the gas cooler $\Delta T_{pinch,\ gc} = T_3 - T_{amb}$ and at the evaporator $\Delta T_{pinch,\ ev} = T_{cool} - T_{10}$ are both assumed to be of 10 [°C] (typically the pinch temperature ranges between 5 and 10 [°C] (Cui et al., 2022)).
- There are no pressure drops across the gas cooler and the evaporator.
- The refrigerant is at saturated vapor state at the evaporator outlet.
- The thermodynamic transformations within the ejector, expansion valve and separator are adiabatic.
- The thermodynamic transformation within the compressor is isentropic. Note that this hypothesis is not true in practice, but this does not constitute the subject of the present analysis for which a simple transformation is sufficient.

Note that the pressure at the gas cooler p_{gc} and at the outlet of the ejector p_{out} are not constrained and those have thus to be imposed in order to solve the system. Based on those hypotheses, the global energy conservation of the system can be expressed as:

$$\dot{Q}_{ev} + \dot{W}_{comp} + \dot{Q}_{gc} = 0, \tag{1}$$

where $\dot{Q}_{ev}$ is the cooling power accumulated by the evaporator, $\dot{W}_{comp}$ is the compression mechanical power and $\dot{Q}_{gc}$ is the heat power discharged at the gas cooler. Also note that in this work the energy introduced into the system is chosen to be positive by convention. From the aforementioned assumptions, Eq. (1) can then be re-written in terms of specific enthalpies:

$$\dot{m}_s(h_{10} - h_9) + \dot{m}_p(h_2 - h_1) + \dot{m}_p(h_3 - h_2) = 0, \tag{2}$$

with $\dot{m}_p$ and $\dot{m}_s$ the primary and secondary mass flow rates, respectively. The number indices on the enthalpy terms (h_i) refer to their position in the cycle (Fig. 1). When dealing with ejectors, an important quantity to monitor is the secondary to primary flow ratio, which is referred to as the entrainment ratio, as the –secondary– flow coming from the evaporator is entrained by the discharged –primary– flow that comes from the gas cooler. The entrainment ratio $\omega = \dot{m}_s/\dot{m}_p$ can then be deduced from Eq. (2):

$$\omega = \frac{h_1 - h_3}{h_{10} - h_8}, \tag{3}$$

where the enthalpy conservation across the expansion valve was used, i.e., $h_9 = h_8$. A similar expression can be found for the COP, for which the general expression, for a cooling cycle, is given by Nehdi et al. (2007):

$$COP = \frac{\dot{Q}_{ev}}{\dot{W}_{comp}}. \tag{4}$$

Much as for ω, the COP can be expressed as a function of the enthalpies:

$$COP = \frac{\dot{m}_s}{\dot{m}_p}\frac{h_{10} - h_9}{h_2 - h_1} = \omega\frac{h_{10} - h_9}{h_2 - h_1} = \frac{h_1 - h_3}{h_2 - h_1}. \tag{5}$$

The cycle can then be fully solved on the basis of the previous assumptions, and the mass conservation equation of the liquid phase at the separator, i.e.:

$$\dot{m}_s = (\dot{m}_p + \dot{m}_s)(1 - x_7), \tag{6}$$

with x the vapor quality. The quality at the inlet of the separator can therefore be expressed as a function of the entrainment ratio only:

$$x_7 = \frac{\dot{m}_p}{\dot{m}_p + \dot{m}_s} = \frac{1}{1 + \omega}. \tag{7}$$

As it is well known, the thermodynamic state of the working fluid is determined by two independent state variables (pressure and temperature are not independent under the saturation dome). To this end, Table 1 summarizes the pair of state variables that are used at each relevant point of the cycle. Then, all other state variables can be retrieved from the equation of state. In the present work, the latter is provided by the COOLPROP library (Bell et al., 2014). The cycle can then be represented in the $p - h$ diagram, as shown in Fig. 2 for typical operation of the ERS. Note that points 4, 5 and 6 are technically

Table 1
Pair of state variables to solve the cycle at each relevant point.

Point	State variable 1	State variable 2
1	$p_1 = p_{out}$	$x_1 = 1$
2	$p_2 = p_{gc}$	$s_2 = s_1$
3	$p_3 = p_{gc}$	$T_3 = T_{amb} + T_{pinch,\ gc}$
7	$p_7 = p_{out}$	$x_7 = 1/(1+\omega)$
8	$p_8 = p_{out}$	$x_8 = 0$
9	$p_9 = p_{10}$	$h_9 = h_8$
10	$T_{10} = T_{cool} - T_{pinch,\ ev}$	$x_{10} = 1$

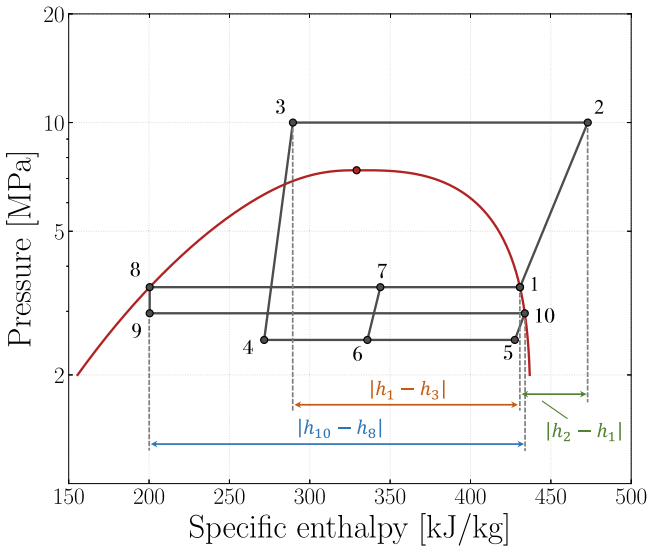

Fig. 2. Classical ERS represented in the $p-h$ diagram. Operating conditions are p_{gc} = 100 [bar], p_{out} = 35 [bar], T_{amb} = 25 [°C] and T_{cool} = 4 [°C] (T_3 = 35 [°C], T_{10} = −6 [°C]). Note that the y axis is in log scale.

within the ejector and correspond to the primary stream at the primary nozzle outlet, secondary stream at the primary nozzle outlet and mixed flow at the secondary throat, respectively (Fig. 1). Fig. 2 allows one to better visualize the enthalpy differences in the expressions of ω and COP in Eqs. (3) and (5), respectively: $\omega = (h_1 - h_3)/(h_{10} - h_8)$, $COP = (h_1 - h_3)/(h_2 - h_1)$.

It is important to mention at this stage that the value of ω predicted by Eq. (3) does not account for any internal mixing phenomenon. Rather, Eq. (3) constitutes the criterion for steady state operation of the cycle as it is derived from the global conservation of energy through the system. In other words, at each set of gas cooler and ejector outlet pressures, a specific value of the entrainment ratio is required by the cycle (determined by Eq. (3)). Therefore, this pseudo ejector model will be referred to as the cycle requirement model in what follows. In this manner, the cycle requirement model can predict the operation of the cycle for any set of operating pressure. Nonetheless, and as it will be seen in Section 3, only specific sets of operating pressures are allowed in an actual ejector cycle.

2.2. Ejector thermodynamic model

As stated previously, the thermodynamic model of Metsue et al. (2022) is used to predict the performance of the real ejector (as opposed to the cycle requirement). This 0D model discretizes the ejector into several section, as seen in Fig. 3, labeled from 0 to d, and the flow is solved at those discrete locations only. The choking of the device is modeled by the compound-choking theory (Lamberts et al., 2018; Metsue et al., 2022), which constitutes the natural condition for the choking of a multi-stream device such as the ejector, as it maximizes the total mass flow rate within the device. The model has already been validated for transcritical CO_2 applications by the authors in Metsue et al. (2021), where the characteristic curves are calibrated on the experimental data of Zhu et al. (2017). The interested reader is invited to review the article of Metsue et al. (2022) for a thorough description of the implementation/validation of the thermodynamic model, as only a brief summary of the model assumptions is presented in what follows. As explained in Metsue et al. (2022), the flow within the system is considered to be one-dimensional, steady, and adiabatic, with negligible velocities at the inlets (primary/secondary) and outlet. To incorporate friction losses along the walls and within the shear layer between the primary and secondary streams, isentropic efficiencies are employed (Fig. 3). These efficiencies include η_p for the primary nozzle (between sections 0 and e), η_{py} for the friction losses encountered by the primary flow within the mixing chamber (between sections e and y), η_s for the friction losses experienced by the secondary flow within the mixing chamber (between sections 0 and y), and η_d for the diffuser (between sections 2 and d). Additionally, mixing losses between the primary and secondary streams are factored in through a loss coefficient η_m (between sections y and m). Furthermore, it is assumed that the primary and secondary streams remain distinct (i.e., no mixing) until they reach a specific section within the constant area duct. At this section, both pressures are considered to be equal, indicating the start of the mixing phenomenon. This section is often referred to as the hypothetical throat in the literature (He et al., 2009). If the ejector operates under a double-choking regime, this section becomes compound-choked. The boundary between single- and double-choking operation of the ejector is then referred to as the critical operating condition or the critical point.

In between each section of the model, the mass and total enthalpy conservation equations are applied. In addition, the equation of state provided by `COOLPROP` and the isentropic efficiency relations (for losses) are used. The momentum conservation equation is also used to handle the mixing, i.e., between sections y and m. In the present work, and as in Metsue et al. (2021), it is chosen to reduce the number of fitting coefficients since some of them have redundant effects on the predicted performance (Metsue et al., 2022). Therefore, it is chosen to set $\eta_{py} = \eta_s$ and $\eta_m = 1$, thus yielding the set of fitting efficiencies at (η_p = 0.95, η_{py} = 0.73, η_s = 0.73, η_m = 1, η_d = 0.85), which have been calibrated on the experimental data of Zhu et al. (2017). Fig. 4 shows the result of the fitting of the ejector model on the experimental characteristic curves reported in Zhu et al. (2017) for transcritical operation. First, η_p is adjusted to fit the primary mass flow rate (the separate values for the primary and secondary mass flow rates are provided in Zhu et al., 2017). Then, η_{py} and η_s are adjusted to match the entrainment ratio at on-design operation, and the position of the off-design part of the characteristic curve is finally adjusted via η_d. In Fig. 4, the efficiencies were tuned to obtain a good fitting for p_{gc} = 9.3 [MPa], and kept constant to generate the curves at p_{gc} = 8.7 and 9.8 [MPa], for which an acceptable fitting ability of the model is also observed. In the following, the efficiencies will thus be kept to those constant values. Note also that no cooling power is specified for the analysis, therefore the size of the component is not relevant and for the ejector, only the throat area ratio (TAR) A_y/A_t, with A the section area, is necessary to solve the system. To this end, a base TAR is chosen as the one of the ejector of Zhu et al. (2017): A_y/A_t = 6.25. This base TAR will be later optimized in Section 3.3. Moreover, the primary nozzle of the ejector of Zhu et al. (2017) is converging only, meaning that $A_e = A_t$. Nonetheless, the influence of A_e/A_t will be discussed in Section 3.3 as well.

3. Results and discussion

In this section, it is proposed to analyze the operation of the classical ERS by combining the approaches presented in Sections 2.1 and 2.2. This allows to both shed light onto the optimal and physically possible operating point of the cycle, as well as to determine what ejector TAR best suits the system, depending on the ambient temperature.

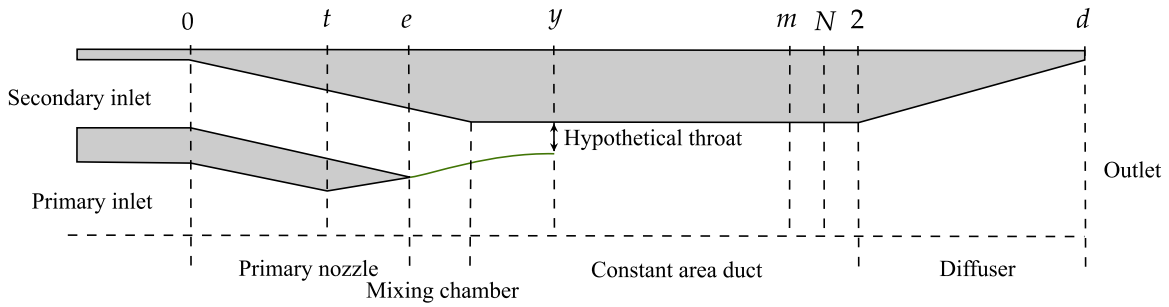

Fig. 3. Schematic of the ejector model, after Metsue et al. (2022).

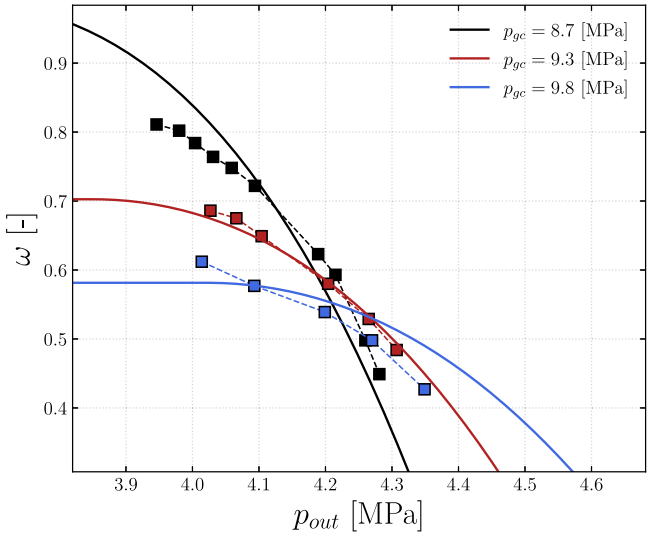

Fig. 4. Fitting of the ejector model onto the experimental data of Zhu et al. (2017) (η_p = 0.95, η_{py} = 0.73, η_s = 0.73, η_m = 1, η_d = 0.85). The experimental data are shown with squares and the thermodynamic model predictions in plain lines.

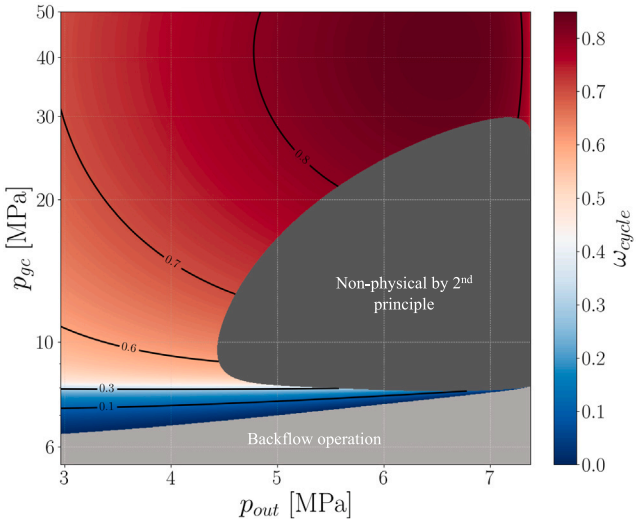

(a) ω required by the cycle (cycle requirement model)

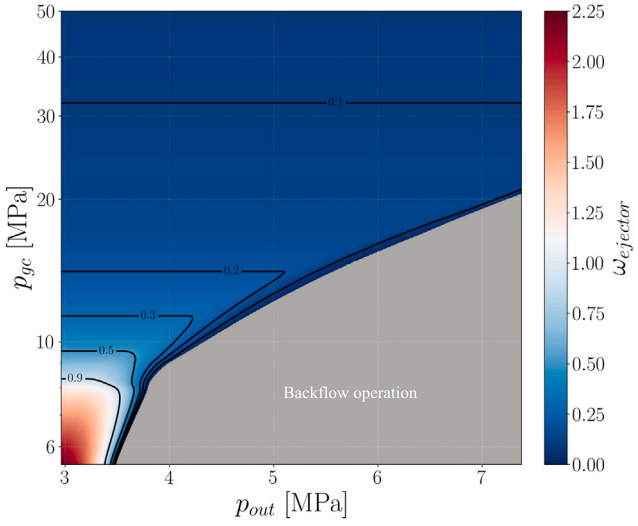

(b) ω predicted by the real ejector model (A_y/A_t = 6.25)

Fig. 5. Maps of the entrainment ratio ω as a function of the gas cooler pressure p_{gc} and the ejector outlet pressure p_{out} for T_{amb} = 25 [°C] (T_3 = 35 [°C], T_{10} = −6 [°C]). Iso-ω lines are plotted in black.

3.1. Entrainment ratio maps

As a first step, it is proposed to compare the entrainment ratios calculated using the two approaches, i.e., using the cycle requirement model (Section 2.1) and the real ejector model (Section 2.2). This is done by building maps of ω as a function of the pressure at the outlet of the ejector p_{out} and the pressure at the gas cooler p_{gc}. The maps boundaries for said pressures are set as follows:

$$\begin{aligned} p_{out} &\in \left[p_{10},\ p_{crit}\right], \\ p_{gc} &\in \left[p_{down},\ p_{up}\right], \end{aligned} \tag{8}$$

where the *crit* subscript refers to the critical conditions (p_{crit} = 7.37 [MPa]). The boundaries for p_{gc} (p_{down} and p_{up}) are free and are thus set as inputs. In the present work and without additional mention, the boundaries are set as (p_{down} = 5.5 [MPa], p_{up} = 50 [MPa]), which is deemed adequate for the present purpose.

Fig. 5 presents maps of the entrainment ratio using the cycle requirement model (Fig. 5(a)) and the real ejector model (Fig. 5(b)) for an ambient temperature of 25 [°C]. As it can be seen, additional portions of the maps have been discarded (in gray). The light gray regions indicate that the cycle was predicted to operate under backflow mode: under those conditions, the flow goes from point 10 to point 9 (Fig. 1). The dark gray region in Fig. 5(a) indicates that the second principle of thermodynamics is not satisfied, i.e., $(\dot{m}_p+\dot{m}_s)\ s_7 < \dot{m}_p\ s_3+\dot{m}_s\ s_{10}$. From Fig. 5(a), it appears that the entrainment ratio does not vary strongly with p_{out} for gas cooler pressures below 10 [MPa] (typical operation range of ERSs). On the other hand, at constant p_{gc}, the real ejector performance prediction (Fig. 5(b)) indicates a constant ω plateau and a rapid decline as the critical pressure of the ejector is exceeded. Actually, each line of the map (i.e., varying p_{out} at constant p_{gc} in Fig. 5(b))

corresponds to an ejector characteristic curve (as described in Metsue et al., 2022), since all inlet parameters are constant.

3.2. Operation of the ERS

To determine the actual –allowable– operation of the ERS, one must find the locus of operating pressures ($p_{gc} - p_{out}$) that satisfies the matching between the entrainment ratio required by the cycle (Fig. 5(a)) and that provided by the ejector (Fig. 5(b)). This said locus is referred to, in the present work, as the operation curve of the cycle. Practically, the operation curve is determined by calculating the entrainment ratio required by the cycle and that predicted by the real ejector model within the ($p_{gc} - p_{out}$) domain, as in Fig. 5. Then, the difference in terms of entrainment ratio is computed at each point of the domain in order to find the zero, that corresponds, by definition, to the operation curve. Consequently, the operation curve is comprised of all sets of ($p_{gc} - p_{out}$) such that $\omega_{cycle} = \omega_{ejector}$. In this section, the operation curves are studied for three ambient temperatures (15, 25 and 35 [°C]). Note however that in the case of $T_{amb} = 15$ [°C], the cycle is not transcritical since the heat rejection (transformation 2 to 3, Fig. 2) at the hot side takes place at a pressure below the critical pressure.

Fig. 6 shows the COP map for the three selected ambient temperatures. The operation curves of the cycle using the ejector model calibrated on the experiment of Zhu et al. (2017) have been plotted in purple. The green curve corresponds to the operation curve of the cycle obtained by setting all efficiencies of the real ejector thermodynamic model to 1 ($\eta_i = 1$). The dots on the operation curves represent the point of maximum COP. The dotted lines represent the lines of critical operation of the ejector (obtained with the thermodynamic model), separating the on-design regime (on the left) from the off-design regime (on the right). It can be seen that for the three ambient temperatures, the maximum COP point on the purple curve (ejector calibrated on Zhu et al., 2017) is found when the ejector operates under off-design regime. This indicates that from the cycle's perspective, it is preferable to have a slightly higher outlet pressure (or equivalently, compression ratio p_7/p_{10}) even if it comes at the price of having a somewhat lower entrainment ratio (Fig. 5(a)). Notice also in Fig. 6(a) that there appears to be a discontinuity at $p_{gc} = 6.43$ [MPa], which corresponds to the saturation pressure at the gas cooler outlet temperature $p_{sat}(T_3)$ (this case is subcritical, as mentioned previously). Thus, as T_3 is fixed, for $p_{gc} > 6.43$ [MPa], there is a condensation process (transformation 2 to 3 goes through the saturation dome), but for $p_{gc} < 6.43$ [MPa], there is no condensation of the hot refrigerant (point 3 is a gas), leading to the poor performance that may be noticed in that region in Fig. 6(a).

In the case of the operation curves obtained with all $\eta_i = 1$, the maximum COP is found under off-design operation of the ejector only for $T_{amb} = 15$ [°C] (Fig. 6(a)). Interestingly, in Figs. 6(b) and 6(c), the maximum COP point is found when the ejector operates at critical conditions, which is in contradiction with the previous remark. Further analysis then indicates that the maximum COP can be found at critical ejector operation even when all efficiencies are not equal to unity. To this end, Fig. 7(a) shows operation curves for $T_{amb} = 25$ [°C] generated by varying one independent efficiency at a time (by default, $\eta_i = 1$). Plain and dashed curves indicate on-design and off-design operation, respectively. As can be seen, the maximum COP is found at critical conditions not only in the case where $\eta_i = 1$ but also when the expansion processes are non-ideal in the primary nozzle. Actually, the optimal COP being located at critical operation is mostly due to the fact that the off-design part of the ejector characteristic curves becomes very steep as the efficiencies get close to unity. This can be seen in Fig. 7(b), where the characteristic curves are plotted for different configurations of the efficiencies for $p_{gc} = 9$ [MPa]. The η_p efficiency does not modify the sharpness of the transition between on- and off-design regimes, unlike η_s, η_{py} and η_d, which is why the optimal COP for $\eta_p = 0.8$ in Fig. 7(a) is found at the critical conditions as in the case where

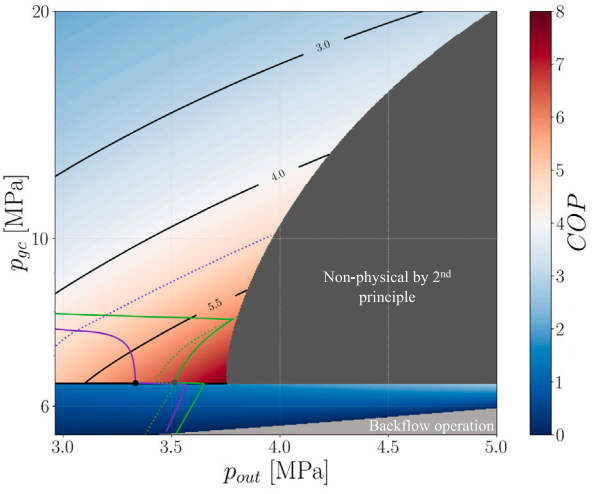

(a) $T_{amb} = 15$ [°C] ($T_3 = 25$ [°C], $T_{10} = -6$ [°C])

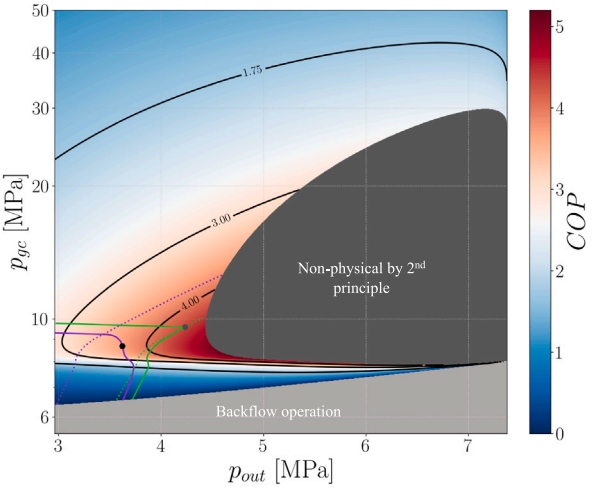

(b) $T_{amb} = 25$ [°C] ($T_3 = 35$ [°C], $T_{10} = -6$ [°C])

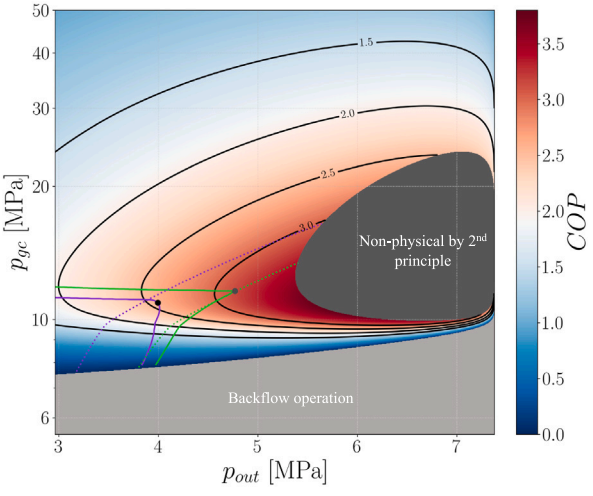

(c) $T_{amb} = 35$ [°C] ($T_3 = 45$ [°C], $T_{10} = -6$ [°C])

Fig. 6. Map of the COP as a function of the gas cooler pressure p_{gc} and the ejector outlet pressure p_{out}. The purple line is the operation curve with the fitting for the ejector of Zhu et al. (2017) and the green line the case with all $\eta_i = 1$. The on-/off-design limit is plotted in dotted lines and the maximum COPs are highlighted with dots.

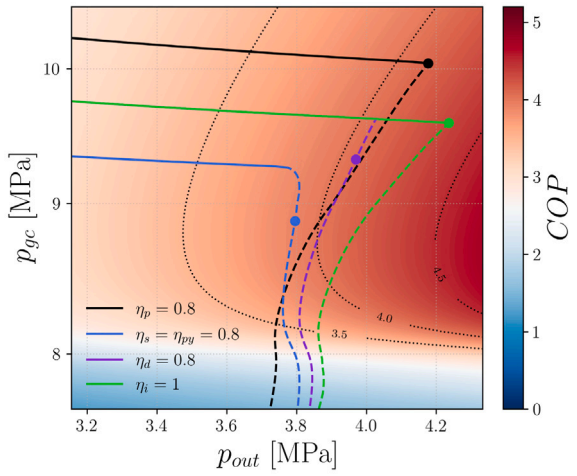

(a) Operation curves

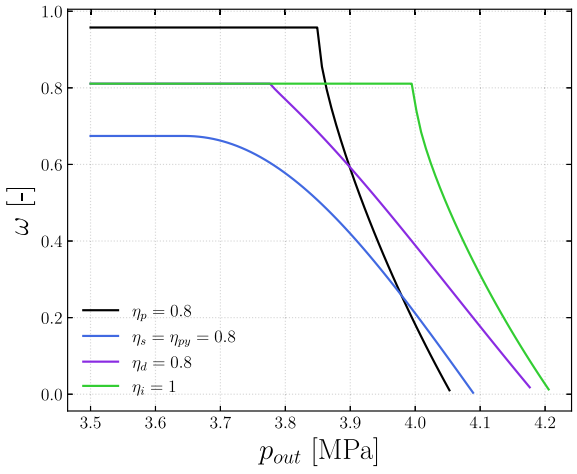

(b) Ejector characteristic curves ($p_{gc} = 9$ [MPa])

Fig. 7. Operation curves and characteristic curves for T_{amb} = 25 [°C] (T_3 = 35 [°C], T_{10} = −6 [°C]) with different sets of efficiencies. Unless indicated otherwise in the legend, all efficiencies are set to unity. In Fig. 7(a), the plain and dashed curves indicate on-design and off-design regime, respectively, and the dotted lines are iso-COPs.

$\eta_i = 1$. The steepness of the characteristic curves translates into a sharp transition between the two regimes in the operation map, as there is a strong decrease in ejector performance as soon as the device goes under off-design. The η_s, η_{py} and η_d efficiencies reduce the sharpness of this transition (Fig. 7(b)) and thereby displace the optimal COP point to the off-design regime of the ejector. From Fig. 6, the highest COP in the maps are found towards the right, at the limit of the non-physical region. Therefore, the best ejector would be one whose operation curve can go as far right of the map as possible (p_{gc} has to be relatively low as well). As per Fig. 7(a), the optimal strategy is then to reduce the entropy generation (have the η_i as high as possible) within the device, as any decrease in one of the efficiencies shifts the operation curve to the left. As a side note, even if all efficiencies are set to unity, entropy is still generated in the modeled mixing process because of the shock waves, which is why the operation curves in Fig. 6 do not reach the limit of the non-physical region (in dark gray). Additionally, it is important to keep in mind that a real ejector always has $\eta_i < 1$, therefore it should be expected that the optimal COP will in practice always be found under off-design operation of the ejector.

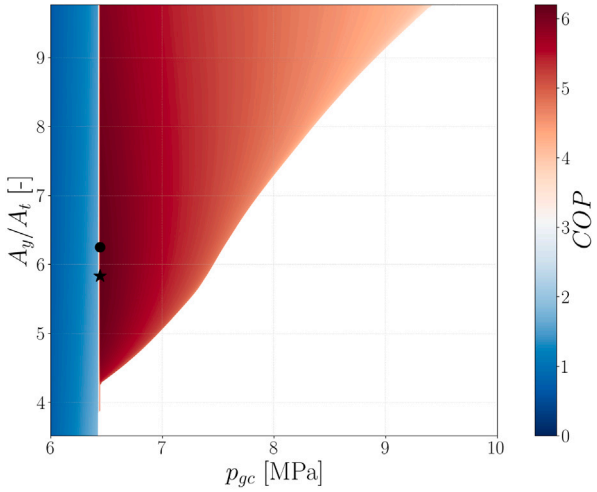

(a) $T_{amb} = 15$ [°C] ($T_3 = 25$ [°C], $T_{10} = -6$ [°C])

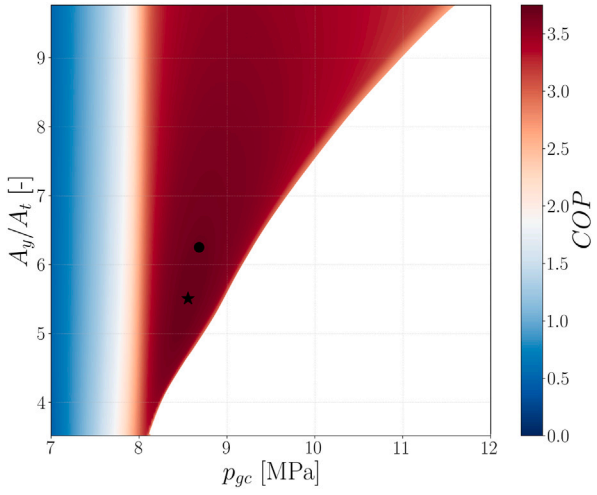

(b) $T_{amb} = 25$ [°C] ($T_3 = 35$ [°C], $T_{10} = -6$ [°C])

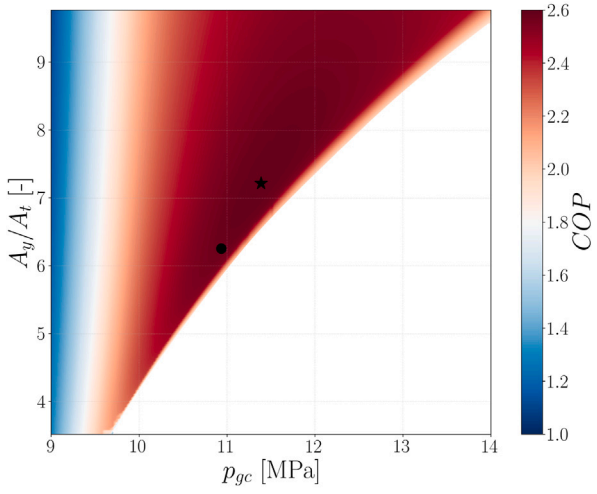

(c) $T_{amb} = 35$ [°C] ($T_3 = 45$ [°C], $T_{10} = -6$ [°C])

Fig. 8. Maps of the COP as a function of the gas cooler pressure and the TAR. The dot and star indicate the locations of the maximum COP with the original geometry of Zhu et al. (2017), and the global maximum COP, respectively.

Table 2
Maximum COP obtainable along the operation curve for the three studied T_{amb} values and for the base (Zhu et al., 2017) and optimal geometries obtained for those temperatures (Fig. 8). Efficiencies are calibrated on Zhu et al. (2017).

Maximum COP	T_{amb} = 15 [°C]	T_{amb} = 25 [°C]	T_{amb} = 35 [°C]
Geom. of Zhu et al. (2017) (TAR = 6.25)	6.17	3.68	2.57
Geom. Optim. for T_{amb} = 15 [°C] (TAR = 5.83)	6.18	3.69	2.55
Geom. Optim. for T_{amb} = 25 [°C] (TAR = 5.50)	6.17	3.70	2.53
Geom. Optim. for T_{amb} = 35 [°C] (TAR = 7.21)	6.12	3.64	2.59

3.3. Influence of the geometry on the COP

As a second step to determine the potentially best operation of the ERS, it is proposed to focus on the impact of the ejector geometry on the ERS performance. To this end, several maps of the COP as a function of the gas cooler pressure and the TAR A_y/A_t are generated. Note that the value of p_{gc} determines a single value of p_{out} along the operation curve (Fig. 6), so that the representation of the COP maps in the space (p_{gc} – A_y/A_t) is unambiguous. It is chosen to focus on the ratio of secondary to primary throat area since it constitutes the main design parameter of the ejector. The primary nozzle exit is first kept equal to the primary throat as in Zhu et al. (2017), Metsue et al. (2021). Note that all maps presented in this section are done with the real ejector model calibrated on the experiment of Zhu et al. (2017). Fig. 8 shows the generated maps for the three studied ambient temperatures. The maximum COP with the original geometry of Zhu et al. (2017) (TAR = 6.25) and the global maximum COP are indicated on the different maps; the global maximum COP being the maximum COP obtained by optimizing the original geometry according to the TAR. The optimal geometry appears to depend on the ambient temperature in a non negligible manner, also implying significantly different operation pressures with respect to the base geometry. Under subcritical operation (Fig. 8(a)), the maximum COP is found at the saturation discontinuity (i.e., at p_{gc} = 6.43 [MPa], as discussed in Section 3.2), which is consistent with Fig. 6(a). In that case, it is then best for point 3 (Fig. 2) to be at saturated liquid conditions (raising or lowering p_{gc} from p_{gc} = 6.43 –at constant T_3– deteriorates the COP).

Table 2 summarizes the maximum COP values indicated in Fig. 8. To estimate the sensitivity to the geometry, the maximum obtainable COP for each of the three optimal geometries (depending on T_{amb}) for each value of T_{amb} is also shown in Table 2. As can be seen, although there is a non negligible difference in optimal TAR depending on the ambient temperature, it appears that the performance gain compared to the base case, or even with respect to the optimal geometry for a different T_{amb}, is marginal. For example, if one were to operate the cycle at T_{amb} = 35 [°C] with the ejector that has the optimal TAR for T_{amb} = 25 [°C], one would only get a decrease in COP of about 2.4% compared to using the optimal TAR for T_{amb} = 35 [°C]. Note however that the TAR should nonetheless lie within a certain acceptable range, as the performance of the ejector may quickly deteriorate (Zeng et al., 2024). Notice that since the optimal TAR does not vary monotonously with T_{amb} (Fig. 8), the maximum COP does not vary monotonously either with the optimal geometries at fixed T_{amb} in Table 2.

Although the TAR seems to have little impact, it is possible that the ejector *size* may play an important role. It is then proposed to determine the ejector dimensions for a fixed cooling power $\dot{Q}_{ev}$ = 30 [kW], but operating at different ambient temperatures. Table 3 summarizes the primary and secondary throat diameters (respectively, D_t and D_y) of the ejector operating at the maximum COP point with the optimized geometry for each T_{amb} (the operating points highlighted by the stars in Fig. 8). As can be seen, the change in dimensions is small from case to case, as there is a difference of less than 0.4 [mm] in primary throat diameter between the extreme cases T_{amb} = 25 [°C] and T_{amb} = 35 [°C]. Such small dimension differences may not justify the implementation of multiple ejector geometries within the ERS and a single geometry that performs relatively well for the range of ambient temperatures of the application could be considered. However, in most refrigeration applications, the required cooling power is not constant, but is rather often directly dependent on the ambient. Then, significant changes in the ejector size are to be expected. For example, if one would operate at T_{amb} = 25 [°C] and the cooling power is reduced from $\dot{Q}_{ev}$ = 30 [kW] to $\dot{Q}_{ev}$ = 15 [kW], the primary throat diameter should, to remain on the maximum COP operation point, be reduced from D_t = 2.76 [mm] to D_t = 1.96 [mm]. For this reason, multi-ejector modules and needle regulated ejectors constitute compelling control technologies. While the first one may contain a discrete number of ejector geometries tailored for specific operating conditions, the latter can precisely regulate the primary mass flow rate, but the TAR is then imposed.

Table 3
Gas cooler pressures, ejector mass flow rates and throat diameters for optimal operation (Fig. 8) at each ambient temperature. The ejector model is calibrated on Zhu et al. (2017).

	T_{amb} = 15 [°C]	T_{amb} = 25 [°C]	T_{amb} = 35 [°C]
p_{gc} [MPa]	6.44	8.56	11.4
$\dot{m}_p$ [kg/s]	0.191	0.245	0.280
$\dot{m}_s$ [kg/s]	0.126	0.131	0.136
ω [-]	0.660	0.534	0.483
D_t [mm]	2.74	2.76	2.39
D_y [mm]	6.62	6.47	6.42

So far, only a converging primary nozzle has been considered. At constant secondary throat area A_y (base geometry), Fig. 9(a) then shows the COP map for T_{amb} = 25 [°C] as a function of the gas cooler pressure and the primary exit to throat area ratio A_e/A_t, with the efficiencies calibrated on Zhu et al. (2017). The white region corresponds to invalid (non physical) predictions of the ejector model. As can be seen, the COP appears to be strongly dependent on A_e/A_t, but this result is actually biased because as A_e gets bigger, the expansion of the primary stream after the throat takes place within the primary nozzle, and $\eta_p > \eta_{py}$ as per the calibration on Zhu et al. (2017). Fig. 9(b) displays a similar COP map but with the η_{py} efficiency now set equal to η_p = 0.95. As can be seen, if one has $\eta_p = \eta_{py}$, the COP becomes strictly independent of A_e/A_t. Nonetheless, the result of Fig. 9(a) still contains some physical insight, since expanding the primary within a diverging part may reduce the entropy generation of this expanding process compared to further expanding it in the mixing chamber, and should lead to an overall higher COP. Actually, it is found that the maximum COP point in Fig. 9(a) (indicated by the star) is located at the limit of the non-physical region, the latter corresponding to a re-compression of the primary stream directly after exiting the primary nozzle, which is not handled by the thermodynamic model. This case (the star) therefore corresponds to having a primary nozzle that can expand the primary stream to the mixing pressure exactly. However, a thorough analysis should be done with CFD tools and therefore exceeds the scope of the present work.

3.4. Analysis of the ejector regime

In this section, it is proposed to analyze the operating regime of the ejector for the base geometry and each of the optimal geometries for the three ambient temperatures of interest (i.e., the same cases as shown in Table 2). To this end, Fig. 10 shows the characteristic curves (ω vs p_{out}) for each case, where the operation points are highlighted with a diamond marker. It can be noticed that all operation points are

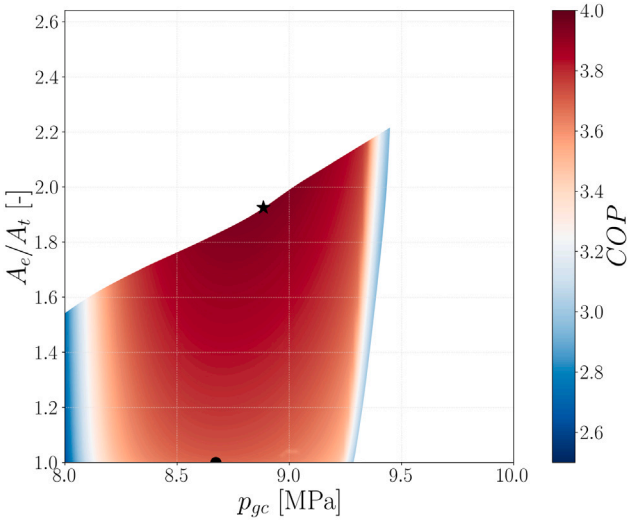

(a) Calibration on [31]

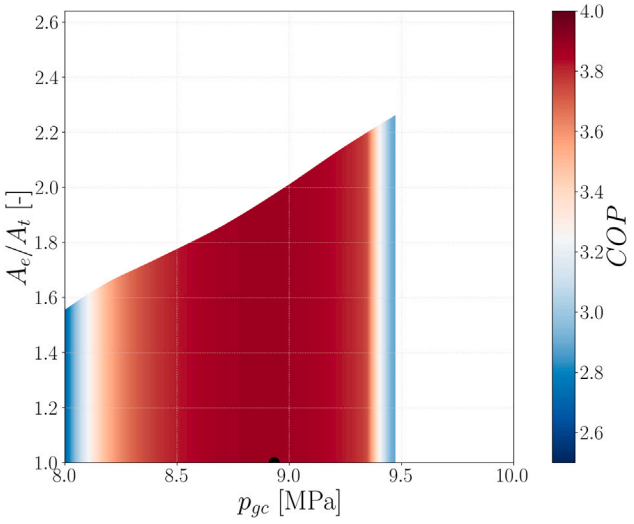

(b) Efficiency η_{py} raised from 0.73 to 0.95

Fig. 9. Maps of the COP as a function of the gas cooler pressure and A_e/A_t for $T_{amb} = 25$ [°C], $T_{cool} = 4$ [°C] ($T_3 = 35$ [°C], $T_{10} = -6$ [°C]). The dot and star (Fig. 9(a)) indicate the locations of the maximum COP with the original geometry of Zhu et al. (2017), and the global maximum COP, respectively.

relatively close to each other for each T_{amb}. In addition, disregarding the case with $\eta_i = 1$, the operation points with higher compression ratios (higher p_{out}) do not necessarily have higher COPs (Figs. 10(b) and 10(c)). Likewise, there is no apparent correlation between how close an operation point is to the critical operation point of the ejector (on-/off-design limit) and the COP. For example in Fig. 10(c), the case with the geometry optimized for $T_{amb} = 35$ [°C] appears to be "more off-design" than the other cases, but actually performs better. The general observation is then that all cases seem to have relatively similar entrainment ratios. One can see in Fig. 10(a) that the case with $\eta_i = 1$ is under far off-design regime, which is a requirement to match the entrainment ratio required by the cycle (Fig. 5). Matching between cycle requirement and ejector performance is the most important factor when designing an ERS, and this requires a non-trivial analysis such as the present one. From this analysis, it is also clear that there is no incentive to operate the ejector under on-design regime for applications where the ejector is used as an expansion device in a refrigeration cycle.

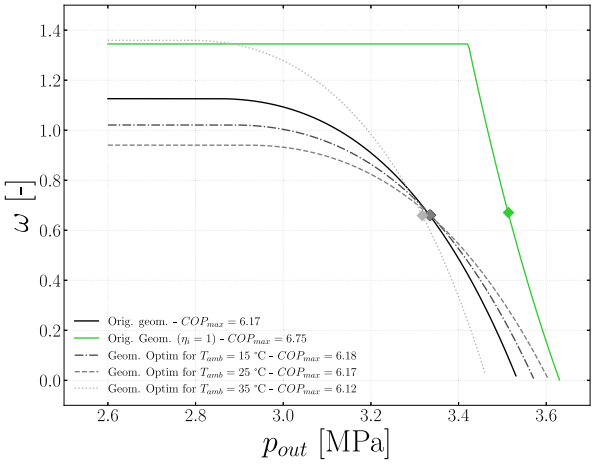

(a) $T_{amb} = 15$ [°C] ($T_3 = 25$ [°C], $T_{10} = -6$ [°C])

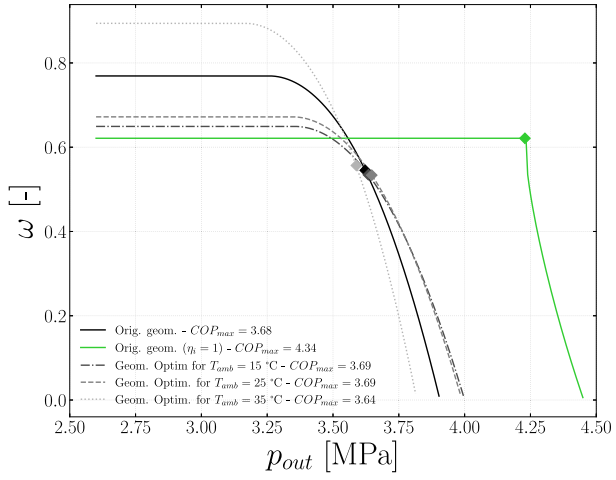

(b) $T_{amb} = 25$ [°C] ($T_3 = 35$ [°C], $T_{10} = -6$ [°C])

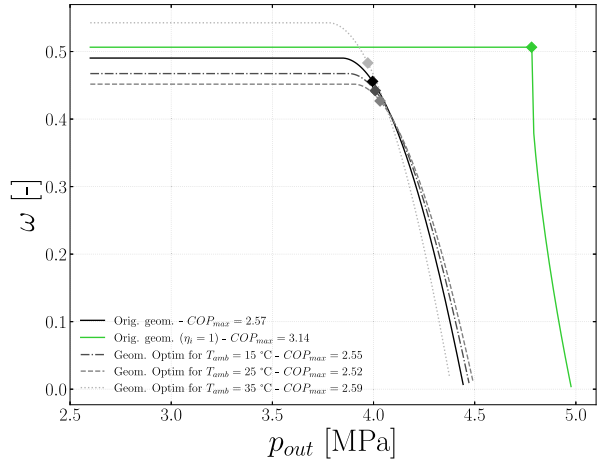

(c) $T_{amb} = 35$ [°C] ($T_3 = 45$ [°C], $T_{10} = -6$ [°C])

Fig. 10. Maximum COP operation points (diamonds) on their characteristic curve for each optimal geometry and for various ambient temperatures. The case with all $\eta_i = 1$ is also shown for reference. The operation points correspond to those in Table 2.

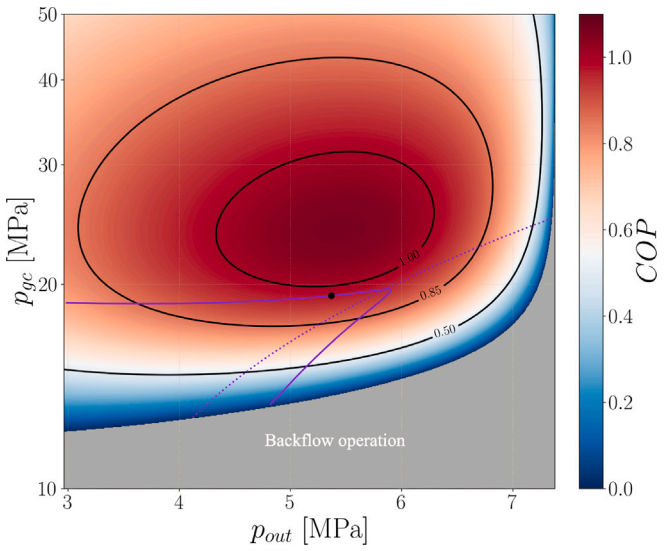

Fig. 11. Map of the COP as a function of the gas cooler pressure p_{gc} and the ejector outlet pressure p_{out} for $T_{amb} = 65$ [°C], $T_{cool} = 4$ [°C] ($T_3 = 75$ [°C], $T_{10} = -6$ [°C]). The purple line is the operation curve with the fitting for the ejector of Zhu et al. (2017). The on-/off-design limit is plotted in dotted line and the maximum COP is highlighted with the dot.

3.5. High temperature gas cooler

So far, the present study indicated that the maximum COP is found when the ejector operates under off-design (or possibly critical) regime. However, it was reported in the work of Metsue et al. (2021) that the optimal operation is found under on-design operation of the ejector, which is in contradiction with the present argument. Actually, despite the cycle configuration being slightly different, the main difference is that the cycle presented in Metsue et al. (2021) is operating as a heat pump to generate heat, not for refrigeration purpose. The hot source temperature is then higher. It is therefore proposed to analyze the operation of the present ERS with a hot source temperature of $T_{hot} = 65$ [°C] (as reported in Metsue et al., 2021). Using the same temperature pinch at the gas cooler as previously, one then gets that $T_3 = 75$ [°C] (Fig. 1).

Fig. 11 shows the generated COP map with the operation curve obtained using the ejector geometry of Zhu et al. (2017) (TAR = 6.25). As in Fig. 6, the dotted line represents the limit between on- and off-design operation of the ejector. As can be seen, the maximum COP point along the operation curve (marked by the black dot) is found within the on-design region, which is in agreement with the conclusions of Metsue et al. (2021). Therefore, based on the present observation along with the previous ones, one can deduce that as T_{hot} gets higher, the maximum COP point gets closer to on-design operation of the ejector (also consistent with Fig. 10) until being found at critical operating conditions at a given temperature. Above said temperature, the maximum COP is found when the ejector operates under on-design regime. In the present configuration of the cycle ($T_{cool} = 4$ [°C] and ejector model calibrated on Zhu et al., 2017), it is found that the switch from on- to off-design regime occurs at $T_{hot} \approx 60$ [°C] ($T_3 \approx 70$ [°C]).

4. Conclusions

In this work, an in-depth theoretical analysis of the operation of the classical ERS was performed using a thermodynamic modeling approach. A state-of-the-art ejector model was integrated within the cycle to generate COP maps and determine both what could be the optimal operation strategy for the cycle, and what would be the main design objectives for the ejector device.

First, it was found that there exists an operation curve, which is the locus of the set of operating conditions that can allow steady state operation of the ERS. This means that, all other parameters being fixed by the application, the cycle cannot operate at any given set of gas cooler and ejector outlet pressures. The allowable sets of pressures are determined by the cycle requirements and the ejector internal physics. Then, the analysis showed that for an ejector with a realistic amount of entropy generation associated to the irreversible mixing phenomena, the maximum COP operation point is likely to be found when the ejector works under off-design regime. As the ambient temperature gets higher, the optimal operation point gets closer to the on-design operation of the ejector and can eventually shift to a full on-design operation if the temperature of heat rejection is higher than a certain threshold.

Secondly, it was found that the main design strategy for the ejector within the ERS is to minimize the entropy generation within the device. Indeed, it was observed that any decrease in any of the efficiencies of the thermodynamic model should lead to a decrease in the maximum achievable COP of the ERS. In addition, it was found that, as entropy generation is reduced within the ejector, the maximum COP point gets closer to critical ejector operation. When the entropy generation becomes sufficiently small, the optimal operation point is found at critical operating conditions of the ejector. However, it was found that there is no benefit to operate the ejector under on-design regime (at pressures lower than that of critical operation regime) for refrigeration applications. In addition, optimizing the throat area ratio of the ejector yielded only little improvement of the COP. It is important to note that constant efficiencies were used to calibrate the ejector model, while it is expected those efficiencies should possibly be functions of the geometry and operating conditions. However, the authors believe that finding such correlations for the efficiencies constitutes a whole subject of research beyond the scope of the present work, certainly requiring the support of machine learning techniques (as in, e.g., Van den Berghe et al., 2023).

From this analysis, it is the authors' understanding that ejector design for refrigeration application should be done by accounting for the whole operation of the system, and not at the component level solely. Note also that the present work is focused on cooling applications, but as established in this paper, above a given hot source temperature threshold, the maximum COP is found when the ejector is under on-design regime, as reported in Metsue et al. (2021). Therefore, a deep analysis of the cycle operating in heat pump mode could be done in the future. Additionally, future work could be done with CFD and machine learning tools to determine the influence of the different 2D/3D geometrical parameters of the ejector, such as, e.g., the primary nozzle divergent angle. This could allow to also support the development of correlations for the fitting efficiencies of the ejector model, or even directly optimize the geometry to minimize the entropy generation within the device.

CRediT authorship contribution statement

Antoine Metsue: Writing – review & editing, Writing – original draft, Software, Methodology, Investigation, Formal analysis, Data curation, Conceptualization. **Hakim Nesreddine:** Writing – review & editing. **Yann Bartosiewicz:** Writing – review & editing, Supervision, Conceptualization. **Sébastien Poncet:** Writing – review & editing, Supervision, Conceptualization.

Declaration of competing interest

The authors declare that they have no known competing financial interests or personal relationships that could have appeared to influence the work reported in this paper.

Acknowledgments

The NSERC chair on industrial energy efficiency established in 2019 with the support of Hydro-Québec, Natural Resources Canada (CanmetEnergy-Varennes) and Copeland Canada Inc. are here gratefully acknowledged. All calculations have been done using the HPC facilities of the Digital Research Alliance of Canada.

References

Abas, N., Kalair, A.R., Khan, N., Haider, A., Saleem, Z., Saleem, M.S., 2018. Natural and synthetic refrigerants, global warming: A review. Renew. Sustain. Energy Rev. 90, 557–569.

Banasiak, K., Hafner, A., Kriezi, E.E., Madsen, K.B., Birkelund, M., Fredslund, K., Olsson, R., 2015. Development and performance mapping of a multi-ejector expansion work recovery pack for R744 vapour compression units. Int. J. Refrig. 57, 265–276.

Bell, I.H., Wronski, J., Quoilin, S., Lemort, V., 2014. Pure and pseudo-pure fluid thermophysical property evaluation and the open-source thermophysical property library CoolProp. Ind. Eng. Chem. Res. 53 (6), 2498–2508.

Van den Berghe, J., Vemula, J., Bartosiewicz, Y., Mendez, M., 2023. A machine learning-based calibration of a 1D ejector model from CFD. pp. 424–435.

Besagni, G., 2019. Ejectors on the cutting edge: The past, the present and the perspective. Energy 170, 998–1003.

Besagni, G., Mereu, R., Inzoli, F., 2016. Ejector refrigeration: A comprehensive review. Renew. Sustain. Energy Rev. 53, 373–407.

Bilir, N., Ersoy, H.K., 2009. Performance improvement of the vapour compression refrigeration cycle by a two-phase constant area ejector. Int. J. Energy Res. 33 (5), 469–480.

Chen, Y., Chen, Z., Chen, Z., Yuan, X., 2021. Dynamic modeling of solar-assisted ground source heat pump using Modelica. Appl. Therm. Eng. 196, 117324.

Cui, Q., Wang, C., Gao, E., Zhang, X., 2022. Pinch point characteristics and performance evaluation of CO2 heat pump water heater under variable working conditions. Appl. Therm. Eng. 207, 118208.

Deng, J.-Q., Jiang, P.-X., Lu, T., Lu, W., 2007. Particular characteristics of transcritical CO_2 refrigeration cycle with an ejector. Appl. Therm. Eng. 27 (2), 381–388.

Elbel, S., Hrnjak, P., 2008. Experimental validation of a prototype ejector designed to reduce throttling losses encountered in transcritical R744 system operation. Int. J. Refrig. 31 (3), 411–422.

Elbel, S., Lawrence, N., 2016. Review of recent developments in advanced ejector technology. Int. J. Refrig. 62, 1–18.

Fangtian, S., Yitai, M., 2011. Thermodynamic analysis of transcritical CO_2 refrigeration cycle with an ejector. Appl. Therm. Eng. 31 (6), 1184–1189.

Gay, N.H., 1931. Refrigerating system, US patent US12490326A.

He, S., Li, Y., Wang, R., 2009. Progress of mathematical modeling on ejectors. Renew. Sustain. Energy Rev. 13 (8), 1760–1780.

Khosravi, A., Koury, R., Machado, L., 2018. Thermo-economic analysis and sizing of the components of an ejector expansion refrigeration system. Int. J. Refrig. 86, 463–479.

Kim, M.-H., Pettersen, J., Bullard, C.W., 2004. Fundamental process and system design issues in CO_2 vapor compression systems. Prog. Energy Combust. Sci. 30 (2), 119–174.

Kornhauser, A.A., 1990. The use of an ejector as a refrigerant expander. In: International Refrigeration and Air Conditioning Conference. Purdue.

Ksayer, E.B., Clodic, D., 2006. Enhancement of CO_2 refrigeration cycle using an ejector: 1D analysis. In: 11th International Refrigeration and Air-Conditioning Conference. Purdue.

Lamberts, O., Chatelain, P., Bourgeois, N., Bartosiewicz, Y., 2018. The compound-choking theory as an explanation of the entrainment limitation in supersonic ejectors. Energy 158, 524–536.

Li, H., Cao, F., Bu, X., Wang, L., Wang, X., 2014. Performance characteristics of R1234yf ejector-expansion refrigeration cycle. Appl. Energy 121, 96–103.

Li, D., Groll, E.A., 2005. Transcritical CO_2 refrigeration cycle with ejector-expansion device. Int. J. Refrig. 28 (5), 766–773.

Liu, F., Deng, J., Pan, W., 2018. Model-based dynamic optimal control of an ejector expansion CO_2 heat pump coupled with thermal storages. Energy Procedia 152, 156–161.

Liu, F., Groll, E.A., Li, D., 2012. Investigation on performance of variable geometry ejectors for CO_2 refrigeration cycles. Energy 45 (1), 829–839.

Liu, F., Qiu, W., Deng, J., Mo, Q., Groll, E.A., Zhao, J., Liang, J., 2020. Multi-objective non-simultaneous dynamic optimal control for an ejector expansion heat pump with thermal storages. Appl. Therm. Eng. 168, 114835.

Metsue, A., Bartosiewicz, Y., Poncet, S., 2021. Investigation on ejector design for CO_2 heat pump applications using Dymola. In: Proc. of the 9th IIR International Conference Ammonia and CO_2 Refrigeration Technologies. International Institute of Refrigeration, Ohrid.

Metsue, A., Debroeyer, R., Poncet, S., Bartosiewicz, Y., 2022. An improved thermodynamic model for supersonic real-gas ejectors using the compound-choking theory. Energy 238, 121856.

Nehdi, E., Kairouani, L., Bouzaina, M., 2007. Performance analysis of the vapour compression cycle using ejector as an expander. Int. J. Energy Res. 31 (4), 364–375.

Pottker, G., Hrnjak, P., 2015. Ejector in R410A vapor compression systems with experimental quantification of two major mechanisms of performance improvement: Work recovery and liquid feeding. Int. J. Refrig. 50, 184–192.

Sarkar, J., 2010. Geometric parameter optimization of ejector-expansion refrigeration cycle with natural refrigerants. Int. J. Energy Res. 34 (1), 84–94.

Singh, S., Hafner, A., Maiya, M., Banasiak, K., Neksa, P., 2021. Multiejector CO_2 cooling system with evaporative gas cooler for a supermarket application in tropical regions. Appl. Therm. Eng. 190 (116766).

Taslimi Taleghani, S., Sorin, M., Poncet, S., 2018. Energy and exergy efficiencies of different configurations of the ejector-based CO_2 refrigeration systems. Int. J. Energy Prod. Manag. 3 (1), 22–33.

Zeng, H., Zhao, H., Zhang, H., Liu, Z., 2024. Simulation study of key cross-sectional area dimensions of CO_2 ejector on performance. Int. J. Refrig. 159, 276–286.

Zhang, Z., Tian, L., 2014. Effect of suction nozzle pressure drop on the performance of an ejector-expansion transcritical CO_2 refrigeration cycle. Entropy 16 (8), 4309–4321.

Zhao, L., Yang, X., Deng, S., Li, H., Yu, Z., 2015. Performance analysis of the ejector-expansion refrigeration cycle using zeotropic mixtures. Int. J. Refrig. 57, 197–207.

Zheng, L., Deng, J., He, Y., Jiang, P., 2015. Dynamic model of a transcritical CO_2 ejector expansion refrigeration system. Int. J. Refrig. 60, 247–260.

Zhu, Y., Li, C., Zhang, F., Jiang, P.-X., 2017. Comprehensive experimental study on a transcritical CO_2 ejector-expansion refrigeration system. Energy Convers. Manage. 151, 98–106.